SCHOOL OF PHYSICS AND ASTRONOMY

YEAR 3 INTERIM PROJECT REPORT

SESSION 2021-2022

Name:	Ashley Thean
Student Number:	C1900846
Degree Programme:	MPhys Physics
Project Title:	Characterizing Arrays of Kinetic Inductance Detectors
Supervisor:	Dr. S Doyle
Assessor	Dr. G Klemencic

Declaration:

I have read and understand Appendix 2 in the Student Handbook: "Some advice on the avoidance of plagiarism".

I hereby declare that the attached report is exclusively my own work, that no part of the work has previously been submitted for assessment (although do note that material in "Interim Report" may be re-used in the final "Project Report" as it is considered part of the same assessment), and that I have not knowingly allowed it to be copied by another person.

Table of Contents

1. Introduction

Kinetic Inductance Detectors (KID) are a type of photodetectors that operate based on the microwave properties of a superconductor. As the name suggests, the response of the detectors is measured from its kinetic inductance, which is a property that emerges from superconductivity.

An incident photon changes the kinetic inductance of the system, and this allows the detection of the photon in a resonant LC circuit which forms the detector, where the change in resonant frequency can be measured and related to the responsivity of the KID.

1.1 Aims and Objectives

The aims of the project are to fully characterise the SFAB Security Imaging System in terms of detector sensitivity and yield. The first step is to understand the microwave properties of superconductors and to relate to how a KID operates. From this, form simple simulations of a KID utilizing microwave properties of superconductors and the Mattis-Bardeen Theory. Following this, data measurements of a KID array can be made, and the data can be analysed to make sensitivity measurements. Finally, compare the data of each detector in the array to the photon noise limit (fundamental minimum noise) of detector and draw conclusions on the noise analysis from observed data.

1.2 Summary of Progress

The project so far has covered the principles of how a KID works, modelling a KID and an outline of how data measurements will be performed to do noise analysis.

Understanding the basics of KIDs included understanding principles of superconductivity and deriving inductances from the Mattis-Bardeen Theory to approximate the effects of temperature on a superconductor. From there, the model of an ideal KID for varying temperatures was made with considerations of microwave electronics readout issues. Using the model, studied the effects of photon detection using the dF_0 formula.

With the basics of KIDs, formulated an outline of how data measurements can be made with an KID to perform analysis on the sensitivity of the focal plane and then measurements of fixed temperatures to characterize the KID. Work on data measurements and concluding the aims specified is planned for the following semester.

1.3 Overview of Supporting Literature

The project is based on a topic that was covered by my supervisor Dr. S. Doyle, therefore principles of KIDs discussed in *Chapter 1* is based on Doyle's Thesis on LEKIDs [1], along with supporting materials [3], [4] and [5]. Non-academic supplementary material [11] and [12] from Doyle also helped understand the workings of the detector.

2. Supporting Theory of KIDs

2.1 Superconductivity in KIDs

2.1.1 Principles of Superconductivity

For superconductors below a critical temperature T_C, the DC resistance falls to zero. The zero resistance can be attributed to a new path for the current through a new density of superconducting electrons, n_s. [1] Bardeen, Cooper and Schrieffer explains this in the BCS Theory [3]. When the temperature decreases below T_C, electrons start to form pairs known as Cooper-pairs with a binding energy of 2Δ. An important property of these pairs is that they do not scatter in the material. This scatter-less property gives rise to zero resistance, which superconductors are known for.

Expanding on this, we can start from the conductivity of normal metals in the Drude Model. Based on Ashcroft and Mermin [4] on the Drude Model, the conductivity of a metal σ_n can be expressed as follows:

$$\sigma_n = \frac{n_n e^2 \tau}{m(1 - j\omega\tau)} \qquad (1)$$

where n_n is normal electron (quasi-particle) density, j equals to $\sqrt{-1}$, e is the elementary charge, τ is the scattering time, m is the mass of the electron and ω is the angular frequency.

Following this, F. London and H. London put forward explanations for the behaviour of electrons in superconductors [5]. As explained, n_s will accelerate in an electric field without being scattered by the ions in the lattice. Within the Cooper-pairs, there exists no scattering events and therefore $\tau = \infty$. Substituting this value of τ into *equation 1*, the conductivity for n_s becomes:

$$\sigma_s = -j\frac{n_s e^2}{\omega m} \qquad (2)$$

This gives us a relationship between n_s and the superconducting conductivity σ_s, which only comprises of an imaginary part that will be further explained in the Two Fluid Model.

2.1.2 Meissner Effect

Another important property of superconductivity is the Meissner effect, where the bulk of the material expels any magnetic field or displays complete diamagnetism [5]. For a perfect conductor, when an external magnetic field is applied, it will work to prevent a change in magnetic field $\dot{B}$. This is given by:

$$\dot{B}(x) = \dot{B}(a)\exp\left(\frac{-x}{\sqrt{m/\mu_0 n_s e^2}}\right) \qquad (3)$$

However, London [5] explains that superconductors display complete diamagnetism and cannot be modelled as perfect conductors. London's solution was to define an expression for the magnetic field B as a function of distance from the superconducting material surface x. This gives the expression for B for a superconductor:

$$B(x) = B(a)\exp\left(\frac{-x}{\sqrt{m/\mu_0 n_s e^2}}\right) \quad (4)$$

where $B(a)$ is the magnetic field at the surface of the material. *Equation 2 and 4* are collectively known as the London Equations and are not derived from any fundamentals of superconductors but are relations for the observed effects. A complete description will be given by the Mattis-Bardeen Theory.

Within the material surface, the magnetic field will fall to $1/e$ of the value of $B(a)$ when at a distance $\sqrt{m/\mu_0 n_s e^2}$. This distance is known as the London Penetration Depth (LPD) λ_L:

$$\lambda_L = \sqrt{\frac{m}{\mu_0 n_s e^2}} \quad (5)$$

λ_L is used for characterizing the effects of photons on superconductors such as a KID, therefore *equation 5* is crucial as shown in the following section.

2.1.3 Two Fluid Model

Following from the formation of Cooper-pairs below T_C, Gorter and Casimir [6] explains that the 2 electron populations, n_s and n_n gives rise to the Two Fluid Model [6] of superconductors. The model considers that a current in a superconductor will have 2 paths it can propagate, which are the 2 populations. From [1], temperature dependence of ratio n_s/n is given by:

$$\frac{n_s}{n} = 1 - \left(\frac{T}{T_C}\right)^4 \quad (6)$$

$$and$$

$$n_n = n - n_s \quad (7)$$

n_s is inversely proportional to $temperature\ T$, whereas n_n also falls due Cooper-pair formation. This relationship can be observed in the graph:

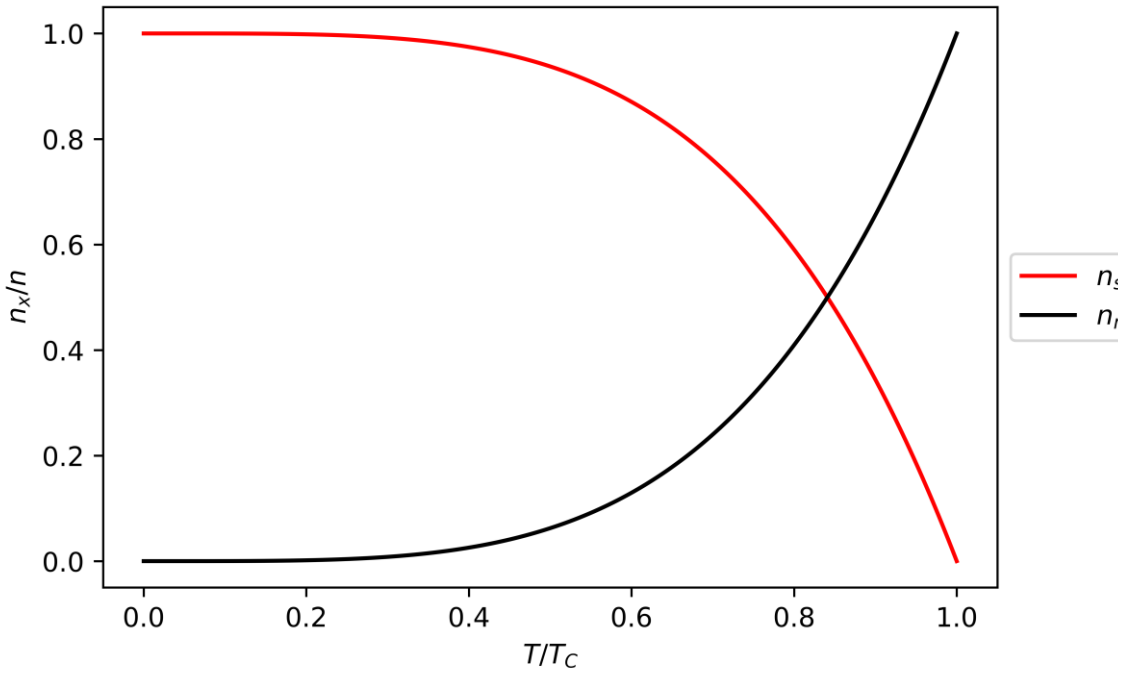

Figure 1 *Graph of ratio of n_s and n_n to total electron population n vs the ratio of temperature T to T_C*

This relationship will be useful in modelling a KID as its response is dependent on the populations [1].

The variation in n_s with temperature means that λ_L also varies with temperature. The expression for λ_L as a function of temperature can be obtained with *equation 5 and 6*:

$$\lambda_L(T) = \lambda_L(0)\left[1 - \left(\frac{T}{T_C}\right)\right]^{-0.5} \qquad (8)$$

where $\lambda_L(0)$ is the LPD at 0K.

For this report, the effects of varying temperature is used to model KID detection. Fundamentally, increasing temperature has the same effect as incident photons, as it provides energy to break Cooper-pairs. The detection of the KID is modelled by temperature changes instead of photon counting as it simplifies the models.

[1] provides an explanation for the effects of varying frequencies incident on a superconducting material; From *equation 2*, at low frequencies σ_s is far greater than σ_n. However, at higher frequencies, especially in the microwave region, σ_n is no longer negligible. This can be attributed to an inertia of n_s as the energy drawn from E is stored as kinetic energy, and this inertia produces a reactance which gives a large impedance at high frequencies. As such, this stored kinetic energy relates to the kinetic inductance of n_s. The effect also causes the current $\boldsymbol{J}_s$ to lag $\boldsymbol{E}$ by $90°$, which explains why σ_s only comprises of an imaginary part. This increase in σ_n with σ_s decrease leads to a larger proportion of $\boldsymbol{J}$ flowing through the resistive quasi-particle path at higher frequencies. This can be illustrated in a circuit-equivalent diagram in *Figure 2*:

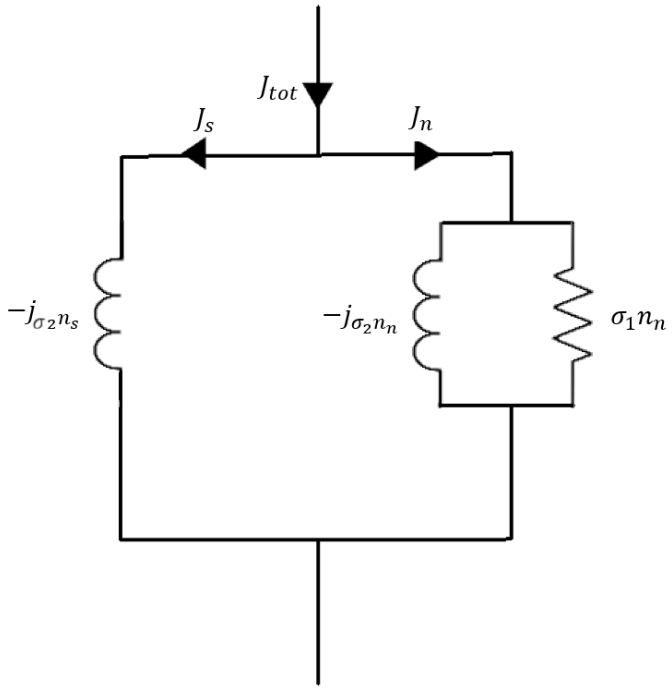

Figure 2 *Circuit-equivalent diagram of current density J through 2 electron densities n_s and n_n at high frequencies*

For a KID, the superconducting path is important as its changes in inductance can be characterised to give information on the detection.

2.2 Internal Inductances

A KID measures a detection through a change in the internal inductance. Building on previous sections, [1] explains that the inductances of a superconducting material can be characterized as it changes with temperature as does λ_L. Kinetic inductance is associated with the kinetic energy of n_s and magnetic inductance L_m is due to the magnetic field energy density by J_s stored in the volume. The derivation is length and beyond the scope of the project, as such we quote [1] for the inductance expressions. The expression for L_k:

$$U_k = \frac{1}{2} L_k I^2 = \frac{1}{2} \mu_0 \lambda^2 \oint J_s^2 \, ds \qquad (9)$$

where I is current and λ is the LPD.

The surface integral that is performed over the cross-section of the strip considers the non-uniform current distribution. Considering the variations in $J_{s,}$ the surface integral can be evaluated and the expression for L_k quoted [1]:

$$L_k = \frac{\mu_0 \lambda}{4\mathrm{W}} \left[\coth\left(\frac{t}{2\lambda}\right) + \left(\frac{t}{2\lambda}\right) \mathrm{cosec}^2\left(\frac{t}{2\lambda}\right)\right] \qquad (10)$$

where t is the thickness and W is the width. The magnetic inductance L_m can also be found with a similar procedure, and the expression was quoted [1]:

$$L_m = \frac{\mu_0 \lambda}{4\mathrm{W}} \left[\coth\left(\frac{t}{2\lambda}\right) - \left(\frac{t}{2\lambda}\right) \mathrm{cosec}^2\left(\frac{t}{2\lambda}\right)\right] \qquad (11)$$

L_k and L_m are in per unit length; by setting length = W, the W term can be eliminated from *equations 10 and 11,* giving in per unit square. The internal inductance L_{int} is simply the sum of the inductances. Quoting from [1]:

$$L_{int} = L_k + L_m = \frac{\mu_0 \lambda}{2} \coth\left(\frac{t}{2\lambda}\right) \qquad (12)$$

where L_{int} is in per unit square.

Equations 10, 11 and 12 are used to model a KID since a change in inductance indicates a detection, λ varies as the temperature varies, as described by $\lambda_L(T)$ in *equation 8*.

Using *equation 10, 11 and 12*, we can generate models of how the L_{int} varies with thickness:

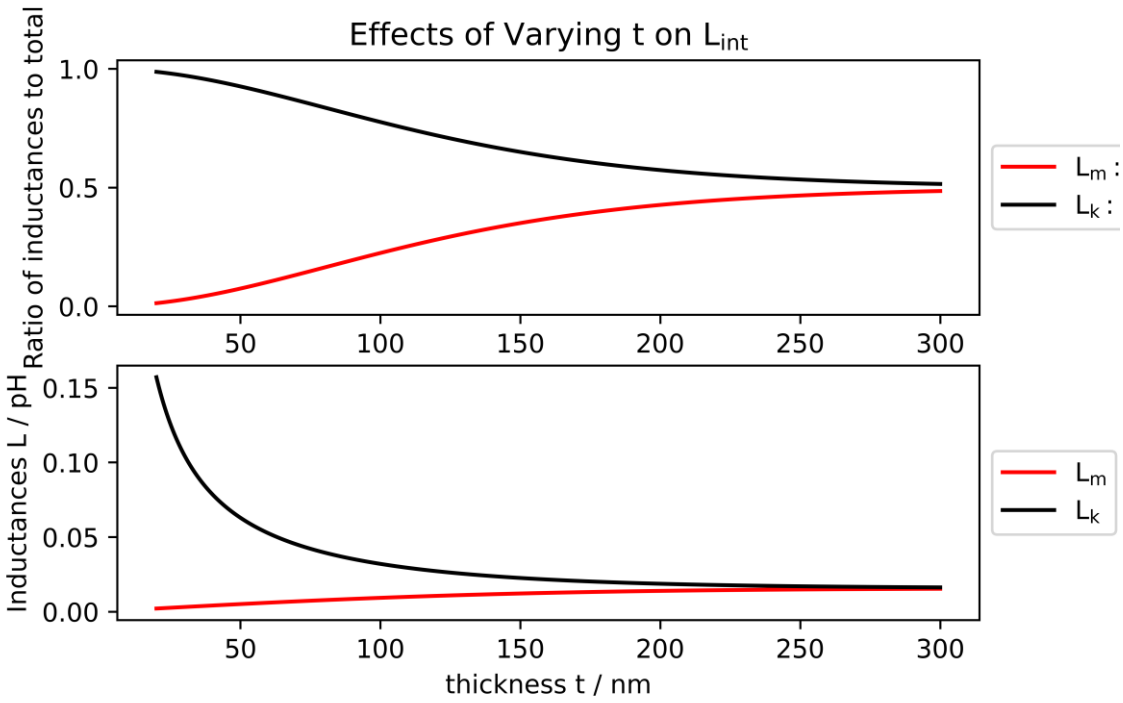

Figure 3 *(Top) Ratios of L_m and L_k to L_{int}. (Bottom) L_m and L_k in pH per square. Both plots were created using a fixed $\lambda = 50nm$*

This relationship will be useful, as [1] shows that $dL_{int}/d\lambda$ varies with thickness; as dλ represents a change in temperature from *equation 8* and L_{int} represents the detection, the sensitivity of the KID is therefore dependent on the thickness. This will be explored in a future section discussing the sensitivity of KIDs.

2.3 Mattis-Bardeen Theory

As mentioned earlier, the results derived for the conductivity is not based on any fundamentals of superconductivity. In BCS Theory [3], the band gap is not introduced and the electrons are accelerated independently if E applied whereas due to finite size of Cooper-pairs, it is not the case. The expressions derived previously holds very well under experimental conditions, but to study the underlying properties of a KID, it would be useful to use expressions for conductivity that consider the band gap and non-local treatment of Cooper-pairs.

Pippard [7] gives a non-local treatment of the London Equations and combined with the band gap, the full effects of the above-mentioned properties lead to the Mattis-Bardeen Approximations for within the limit $k_B T \ll \Delta(0)$ [8]:

$$\frac{\sigma_1}{\sigma_n} = \frac{2\Delta(T)}{\hbar\omega}\exp(-\Delta(0)/k_B T)K_0(\hbar\omega/2k_B T)[2\sinh(\hbar\omega/2k_B T)] \qquad (13)$$

$$and$$

$$\frac{\sigma_2}{\sigma_n} = \frac{\pi\Delta(T)}{\hbar\omega}[1 - 2\exp(-\Delta(0)/k_B T)\exp(-\hbar\omega/2k_B T)I_0(\hbar\omega/2k_B T)] \qquad (14)$$

I_0 and K_0 are the modified Bessel functions of the first and second kind respectively. $\Delta(T)$ is the temperature dependent binding energy, and $\Delta(0)$ is the binding energy at $0\ K$. The derivations and underlying theories are beyond the scope of this project, only the conductivity expressions are important.

$\frac{\sigma_1}{\sigma_n}$ and $\frac{\sigma_2}{\sigma_n}$ can be plotted against T to show the temperature variation using *equation 13 and 14*:

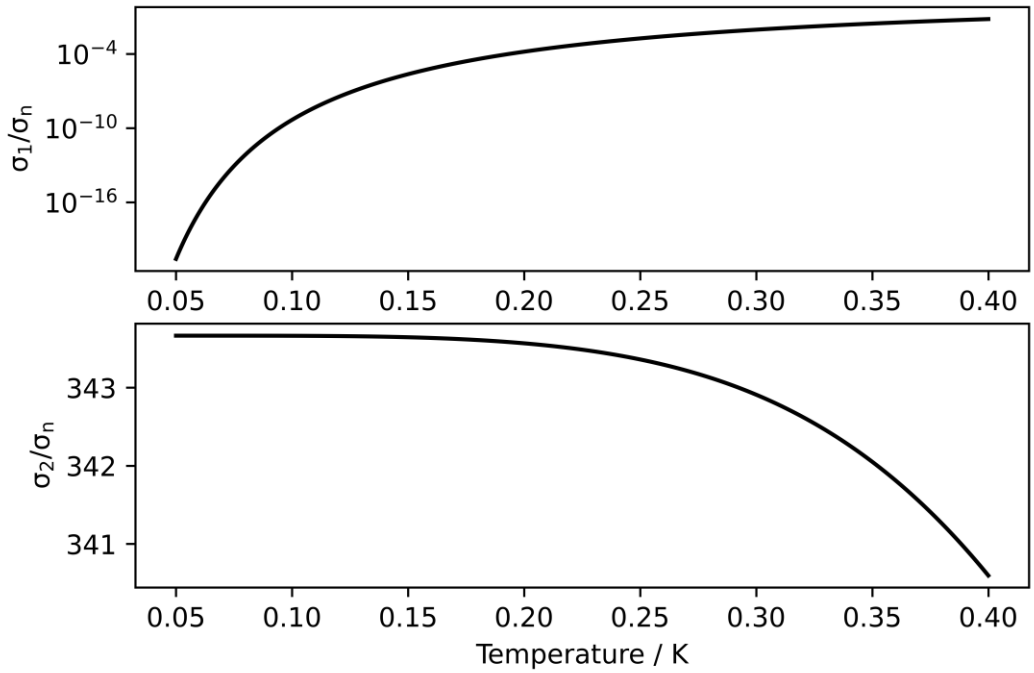

Figure 4 *$\frac{\sigma_1}{\sigma_n}$ and $\frac{\sigma_2}{\sigma_n}$ against T for an Aluminium sheet at 7GHz*

σ_1 can be observed to increase and σ_2 decreases with increasing T, which agrees with the Two Fluid Model as Cooper-pairs break.

By using σ_2 from the Mattis-Bardeen Approximations, combined with the real part of *equation 2* for σ_2 and *equation 5* for λ, the Mattis-Bardeen LPD $\lambda_{MB}(T)$ is found:

$$\lambda_{MB}(T) = \sqrt{1/(\mu_0 \sigma_2 \omega)} \qquad (15)$$

Using *equation 13,14 and 15*, a graph of L_{int} against T can be obtained:

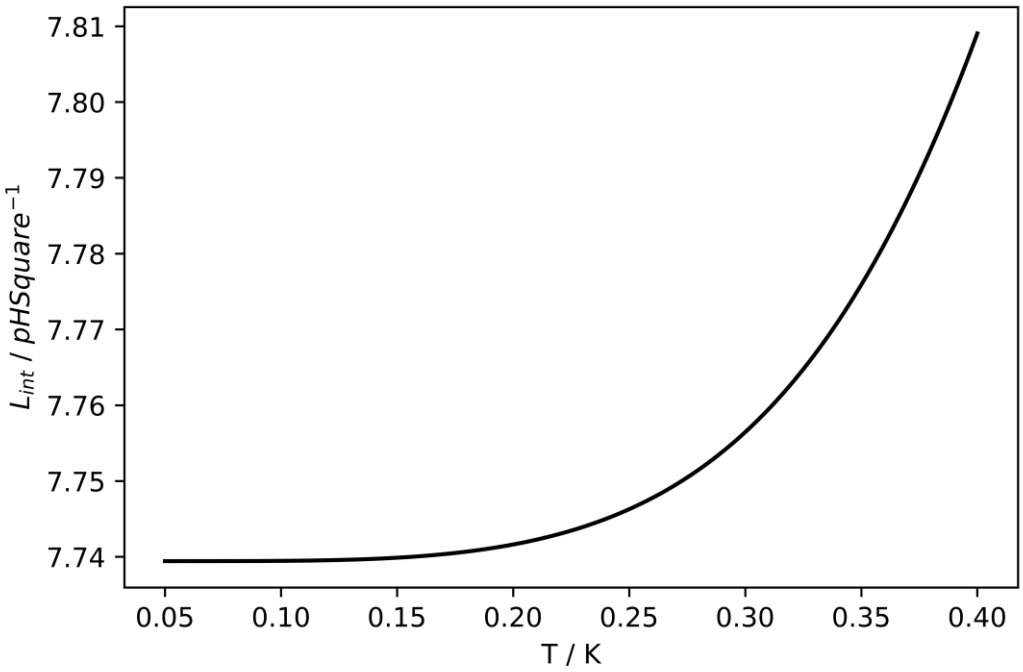

Figure 5 *L_{int} variation with T for an Aluminium sheet at 7GHz using Mattis Bardeen Approximations*

[1] shows that the resistance R of a superconducting strip can then be calculated from the real part of the impedance. Quoting the expression for R from [1]:

$$R = L_k \omega \frac{\sigma_1}{\sigma_2} \qquad (16)$$

Using *equation 14 and 16*, R variation with T can be observed:

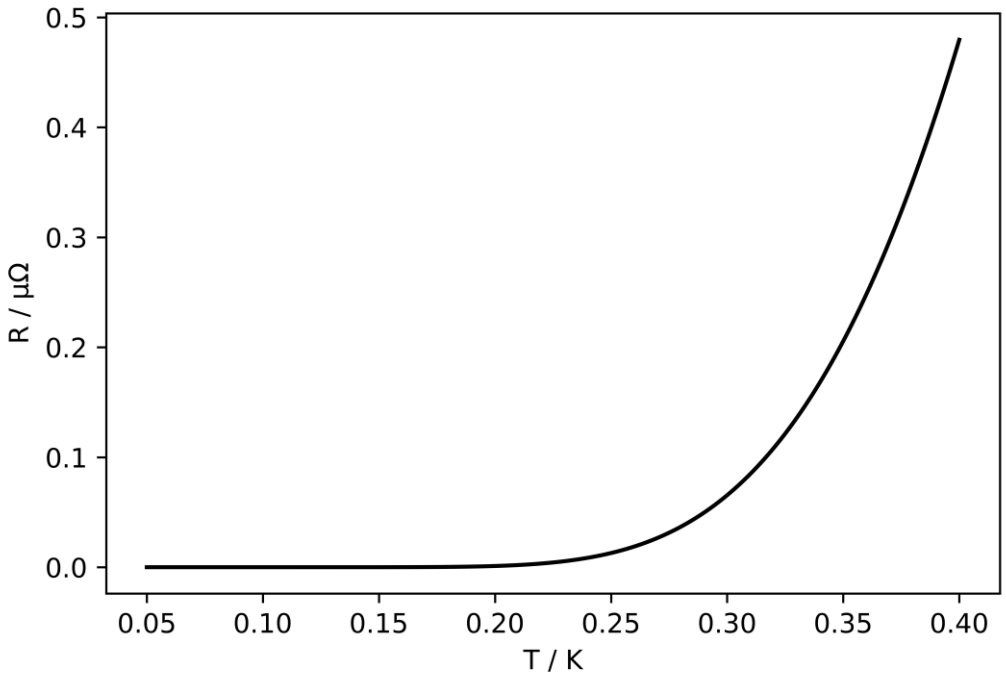

Figure 6 *R variation with T for an Aluminium sheet at 7GHz using Mattis Bardeen Approximations*

The variation in R for different T is useful in modelling a KID as the resistance gives the loss of the detector. The result of this will be explored in the Ideal KID Model section.

2.4 Kinetic Inductance Detector

Schematic

With all the fundamentals established, it is now possible to define a KID. The detection of photons is accomplished on a KID Resonant Circuit. It is a circuit that sits on an aluminium sheet along with a silicon wafer that acts as the ground [11]. A schematic is shown below:

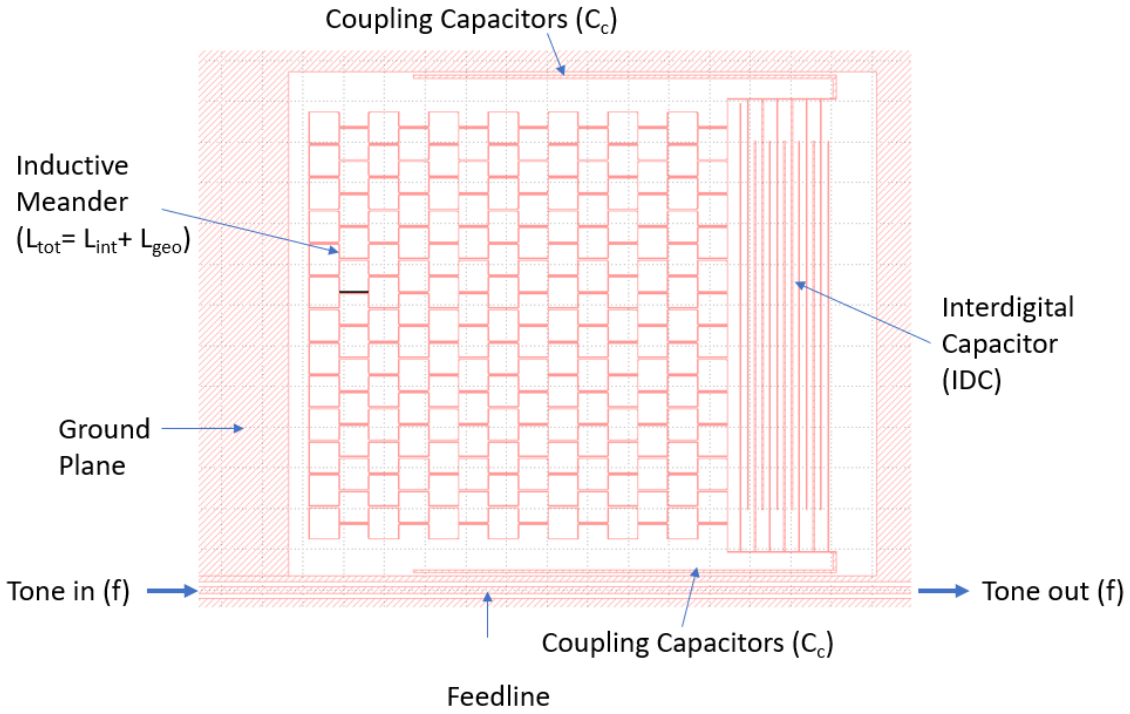

Figure 7 *Schematic of a single KID, with an aluminium sheet (Dashed) which contains the circuit on a silicon ground plate (White) (Image from [12])*

The detector operates at $250 - 300\ mK$ [1], well below T_C; as we will see later that lower system temperatures lead to lower circuit-noise contribution and more accurate readouts. The inductive meander has a total inductance $L_{tot} = L_{int} + L_{geo}$, which is coupled to the interdigital capacitor IDC. L_{geo} is the geometric inductance, that is dependent on the dimensions and material of the meander, its derivation is beyond the project and since the KID dimensions and material remain constant, L_{geo} remains constant and will be taken as such. The circuit behaves as an LC circuit that has resonant frequency ω_0. The diagram can be illustrated as a circuit diagram as shown in *Figure 10* below:

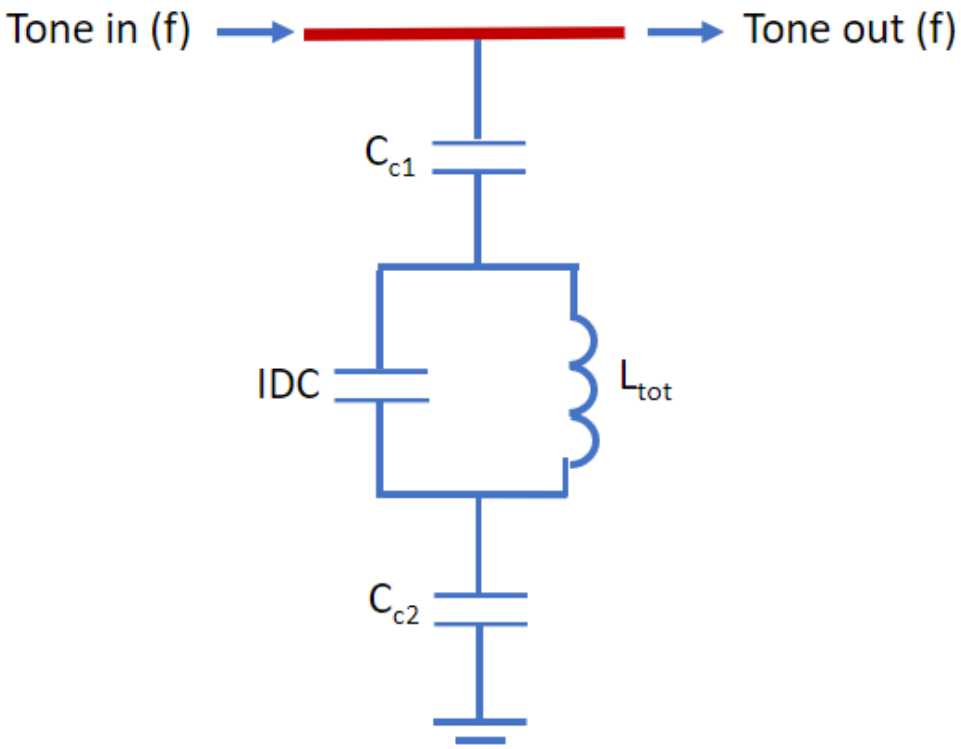

Figure 8 *Circuit diagram of the KID resonant circuit where L_{tot} is the inductive meander (Image from [12])*

There are 2 coupling capacitors, the first coupling capacitor C_{c1} is coupled to the transmission feedline and the second C_{c2} is coupled to ground. [11]

When a photon is incident on the detector, it provides energy for Cooper-pairs to overcome Δ. n_s decreases as Cooper-pairs break, and therefore L_{int} will vary according to *equation 12* and therefore L_{tot} varies as well.

The capacitance C_c of the coupling capacitors and the total capacitance C_{tot} is given [11]:

$$C_c = \frac{C_{c1}C_{c2}}{C_{c1} + C_{c2}} \qquad (17)$$

\

$$and$$

$$C_{tot} = IDC + C_c \qquad (18)$$

As mentioned, the circuit is modelled as an LC circuit with a resonant frequency [11] that can be found from C_{tot} from *equation 18* and L_{geo}:

$$\omega_0 = \frac{1}{\sqrt{L_{tot}C_{tot}}} \qquad (19)$$

Since L_{tot} varies with respect to photon intensity incident on the inductive meander, ω_0 varies accordingly. ω_0 is coupled to the transmission feedline, thus a change in the frequency can be measured.

Microwave Electronics Readout

[11] explains a common phenomenon faced by microwave electronics, such as KIDs, where electronic components' dimensions become comparable to signal wavelengths. Due to this, signals might be out-of-phase when reading out leading to an error. Therefore, treatment of the signal must be of a wave instead of voltage and currents. An illustration is shown below:

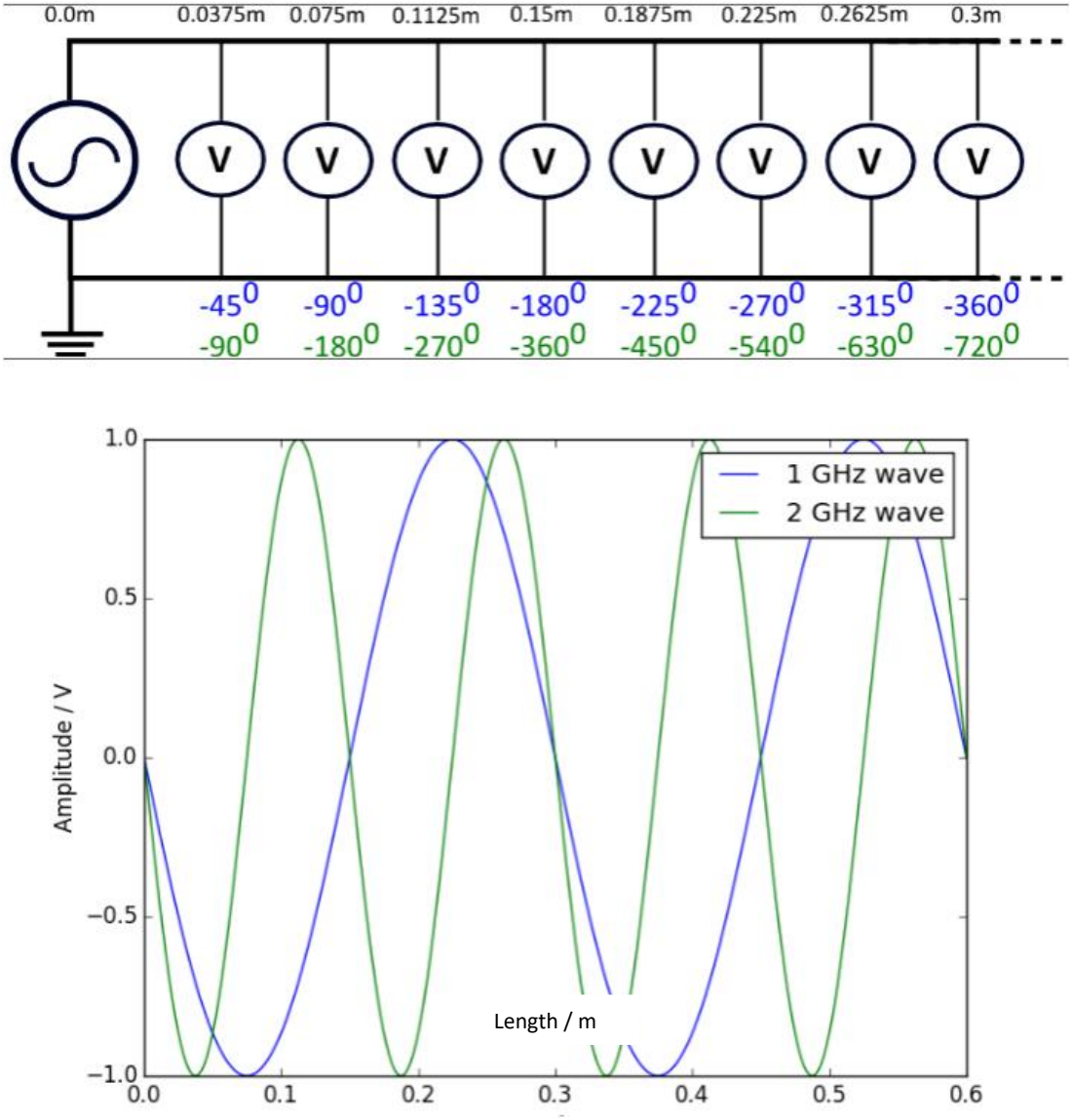

Figure 9 *Diagram illustrating phase difference of microwave frequency readouts at different length of a wire (Image from [12])*

As such, it is useful to define a microwave circuit based on the scattering parameters. Scattering parameters is defined as the ratio of voltages on 2 ports [10]. For a KID it is the ratio of input signal through the feedline into the KID to its respective output signal. A circuit-equivalent diagram of a single KID on a transmission line is shown:

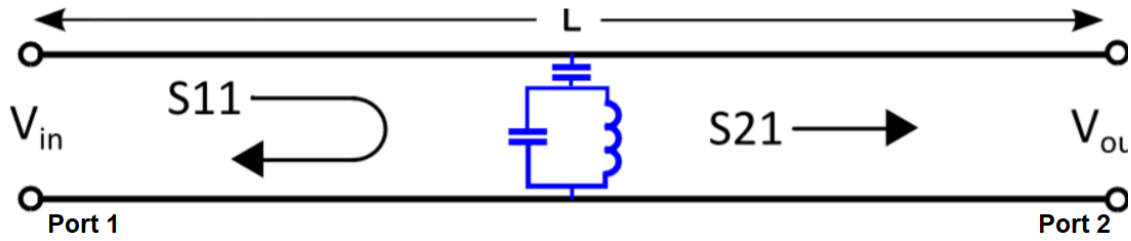

Figure 10 *Schematic of a single KID on a transmission feedline with the blue section representing a KID resonant circuit (Image from [11])*

The scattering parameter that gives the change in ω_0 is S21. Its derivation is beyond the scope of this project, therefore the expression for S21 is quoted from [11]. S21 is a complex number, it would be intuitive to express this as an amplitude $|S21|$ and phase ϕ_{s21}. These values are given [11]:

$$|S21| = \sqrt{Q^2 + I^2} \tag{20}$$

and

$$\phi_{s21} = \text{Arctan}(\frac{Q}{I}) \tag{21}$$

where I and Q is the real and imaginary component of S21 respectively. A KID will measure and output I and Q values in units of Volts. We can use the above expressions to characterize the measurements.

2.5 Ideal KID Simulation

Combining the microwave properties of superconductors and the KID resonator circuit readout, it is now possible to model a KID with temperature variation, corresponding to a detection. The model was created using Python with several values quoted as constant parameters for a superconducting aluminium sheet:

- $L_{geo} = 55.6 \times 10^{-9}\ H$
- $Tone\ Freqeuncy\ F_0 = 0.95\ GHz$
- $Number\ of\ squares\ =\ 27223$
- $C_c = 1.5 \times 10^{-14}\ F$
- $Critical\ Temperature\ of\ Aluminium\ Sheet\ T_c = 1.5\ K$
- $Normal\ State\ Conductivity\ of\ Material, \sigma_n = 6.0 \times 10^7\ \Omega^{-1}m^{-1}$
- $Thickness\ of\ Superconducting\ Sheet, t = 20\ nm$

The $\Delta(0)$ is defined as follows [1]:

$$\Delta(0) = \frac{3.5 k_B T_c}{2} \qquad (22)$$

$\Delta(T)$ approximated to $\Delta(0)$ as a fixed value since dT is small and has insignificant changes to $\Delta(T)$.

The model was created with the following steps:

1. From *equation 13 and 14,* the Mattis-Bardeen Approximations can be found for σ_s and λ can be found from the expression for LPD using equation 8.
2. Using the *equation 10, 11 and 12* for the inductances, the temperature variation of L_{int} can be found and therefore L_{tot} was found after.
3. Using the resonant circuit *equation 19,* ω_0 was found along with |S21|
4. Using *equation 16*, determine variation in the resistive part R with temperature, which increases the loss as temperature increases.

The resulting plot is as follows:

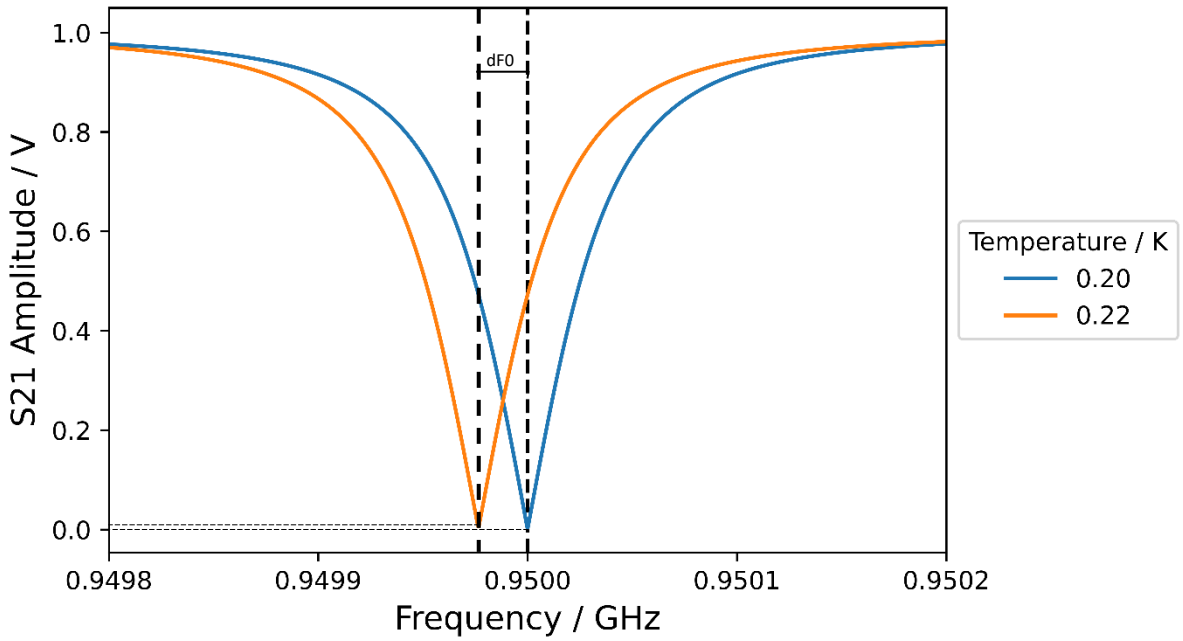

Figure 11 *Tone Frequency variation of a single KID for 2 temperatures with the fixed parameters given above, with dF0 labelled. For real measurements, plots like these where |S21| plotted against frequency is known as Sweep data/plots.*

The shift in tone frequency, dF_0 for the minimum of |S21| corresponds to photon detection as increasing temperature changes F_0. This will be characterized further in the responsivity section. In a constant R system, the |S21| does not vary with temperature and will be the same as the base temperature (lowest), the increase is due to varying R contributing to loss.

An intuitive way of understanding the I and Q variations (measured quantities) is by plotting I vs Q for varying temperatures, given below:

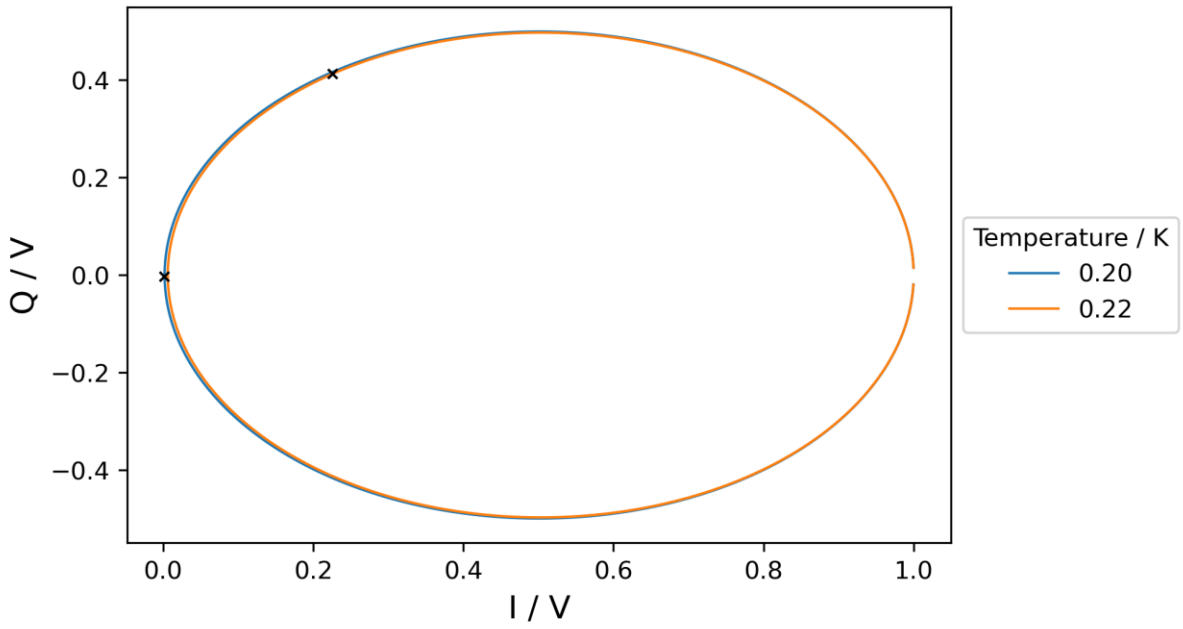

Figure 12 *I vs Q plot for 2 temperatures. The crosses represent the I and Q values corresponding temperature plot at* F_0.

Figure 12 shows the shift I and Q for different temperature, where the cross represents a shift in I and Q at frequency F_0. In real KID measurements, the data typically consists of I and Q values for both the sweep and time-steams (across time) for a set tone frequency F_0 *Figure 12* illustrates how the I and Q values vary at the tone frequency, and ∂F_0 can be related to the response of the detector.

[11] explains that to characterise ∂F_0, we can utilize a formula that considers $\partial I \; and \; \partial Q$ as they can be found for the change in I and Q (measured quantities) from the base temperature. The formula was quoted [11]:

$$\partial F_0 = \frac{\partial I(t)\frac{\partial I}{\partial F} + \partial Q(t)\frac{\partial Q}{\partial F}}{\left(\frac{\partial I}{\partial F}\right)^2 + \left(\frac{\partial Q}{\partial F}\right)^2} \qquad (23)$$

where $\partial I(t)$ and $\partial Q(t)$ are the changes in I and Q values for a particular data point. $\frac{\partial I}{\partial F}$ and $\frac{\partial Q}{\partial F}$ can be calculated by taking numerical derivatives at the minimum point of the sweep data at the tone frequency (In the above case, the base temperature).

Equation 23 is crucial, as it makes it possible for the conversion of I and Q measurements of time-stream and sweep data, to changes in F_0. The change in F_0 corresponds to a detection and is important in characterizing the response of the detector. This will allow us to do noise analysis and sensitivity measurements, which will be explored in the experimental section.

Equation 23 holds well for small deviations in F_0, after which the formula starts to deviate from real data. This limit can be observed by plotting the formula along with the minimum of |S21| from the model. This is shown below:

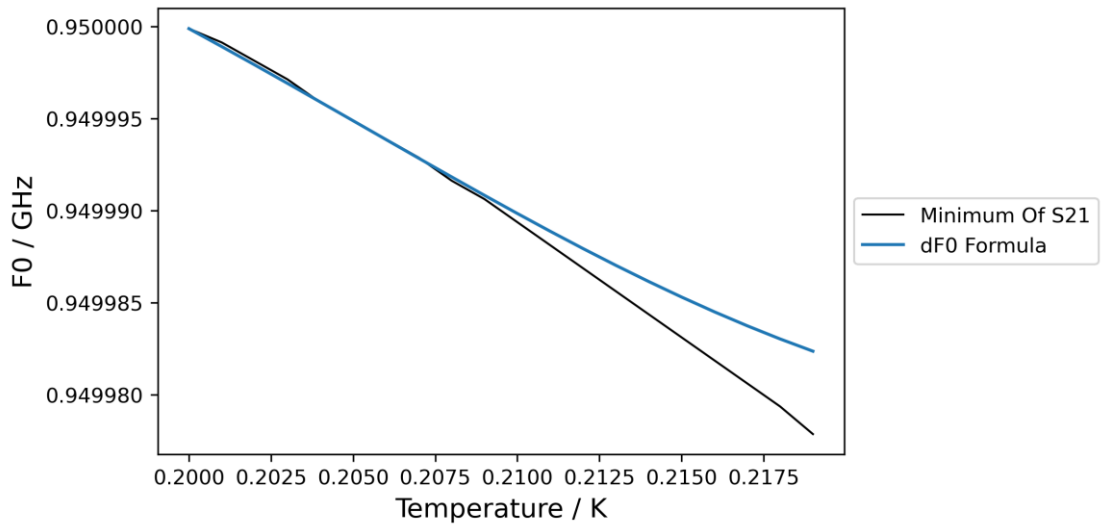

Figure 13 *∂F_0 formula plotted alongside the minimum of |S21| from the model for varying T*

Figure 13 shows that the ∂F_0 formula holds remarkably well up till 0.21K. As such, the ∂F_0 formula is appropriate for low temperature variations, therefore the maximum change in F_0 for the approach to still be valid is $\pm \; 10000Hz$. This is finding imperative as this is the maximum variation that should be taken when doing future measurements.

3. Future Work and Experimental Methods

With the basics of KIDs defined and an ideal model established, the project can now move onto characterizing an array of LEKIDs. In the next semester, the project will work on understanding data measurement methods for an array of LEKIDs using real time-stream and sweep data. Following this, the responsivity of each detector can then be characterised by using known temperature objects and measuring the signal of it. Once the responsivity is characterized, noise analysis can now be performed by analysing real data to show that sensitivity improves.

By increasing the frequency, the sensitivity of the device improves exponentially as generation recombination noise is reduced. As such, the aim is to make sensitivity measurements and to show by comparing the data of each detector to the photon noise limit, that is indeed photon-noise limited.

The experimental methods described below is just an outline and plan for the next semester, and as a brief description of the methods and techniques that will be used.

3.1 Data Measurements and Responsivity for LEKID Array

The LEKID array has measurement outputs of the I and Q values for the frequency sweep and timestream data for each KID. The first step is to use the sweep data, which gives |S21| as a function of frequency that gives the resonant feature of a single KID and determine the largest $\left(\frac{\partial I}{\partial F}\right)$ and $\left(\frac{\partial Q}{\partial F}\right)$.

Using the timestream data which is measured as |S21| as a function of time, the values can then be used in the ∂F_0 formula to determine where to place the tone frequency. Once the timestream data can be characterised, we can move on to characterizing the responsivity of each detector by using the KID to measure known temperature objects, where they will be treated as a blackbody and the output power known; the responsivity will simply be the fraction of $\frac{\partial F_0}{dP}$.

3.2 Noise Analysis and Sensitivity Measurements

Using the timestream data, it is now possible to perform noise analysis and sensitivity measurements. This can be done by taking measurements of well-defined blackbody objects with the temperature known, such as a heated metal bar. The LEKID can scan across the bar and background (the room) the infrared signal can be measured. The noise can be found by “subtracting” the background room frequency from the bar, which gives the optical power of the bar. We can also characterise the other non-trivial sources of noise such as 1/f noise, white noise and others from the detector, which we will go into more detail in the future.

Finally, we can also determine the photon noise limit noise (Fundamental “minimum” noise) of the detector and compare with measured data to characterise it.

4. References

[1] S. Doyle, P. Mauskopf, J. Naylon, A. Porch and C. Duncombe. Lumped Element Kinetic Inductance Detectors. Journal of Low Temperature Physics, 151(1), 530-536, 2008

[2] Porch, A., Mauskopf, P., Doyle, S., & Dunscombe, C. Calculation of the characteristics of coplanar resonators for kinetic inductance detectors. *IEEE transactions on applied superconductivity*, *15*(2), 552-555, 2005

[3] J. Bardeen, L. N. Cooper, and J. R. Schrieffer. Theory of Superconductivity. Physical Review, 108:1175–1204, December 1957

[4] N. W. Ashcroft and N. D. Mermin. Solid State Physics. Saunders College Publishing, 1976.

[5] F. London and H. London. The Electromagnetic Equations of the Supraconductor. Royal Society of London Proceedings Series A, 149:71–88, March 1935

[6] C. J. Gorter and H. Casimir. On supraconductivity I. Physica, 1:306–320, 1934

[7] A. B. Pippard. An Experimental and Theoretical Study of the Relation between Magnetic Field and Current in a Superconductor. Royal Society of London Proceedings Series A, 216:547–568, February 1953.

[8] D. C. Mattis and J. Bardeen. Theory of the Anomalous Skin Effect in Normal and Superconducting Metals. Physical Review, 111:412–417, July 1958.

[9] B. A. Mazin. Microwave kinetic inductance detectors. PhD thesis, California Institute of Technology, United States – California, 2005

[10] D. M. Pozar. Microwave Engineering. Wiley, 2005.

Non-academic Literature

[11] S. Doyle, Understanding Kinetic Inductance Detector Microwave readout, 2021

[12] S. Doyle, Slides explaining Schematics of KID, 2021